Nonlinear Coherent Transport of Waves in Disordered Media

Thomas Wellens[1] and Benoît Grémaud[2]

[1]Institut für Theoretische Physik, Universität Erlangen-Nürnberg, Staudtstrasse 7, 91058 Erlangen, Germany
[2]Laboratoire Kastler Brossel, Ecole Normale Supérieure, CNRS, UPMC, 4 place Jussieu, 75252 Paris Cedex 05, France

(Received 13 July 2007; revised manuscript received 10 October 2007; published 24 January 2008)

We present a diagrammatic theory for coherent backscattering from disordered dilute media in the nonlinear regime. We show that the coherent backscattering enhancement factor is strongly affected by the nonlinearity, and we corroborate these results by numerical simulations. Our theory can be applied to several physical scenarios such as scattering of light in a nonlinear Kerr medium or propagation of matter waves in disordered potentials.

DOI: 10.1103/PhysRevLett.100.033902 PACS numbers: 42.25.Dd, 42.65.−k

The interplay between disorder and—even very weak—nonlinearity can lead to dramatic changes to the system's properties: for example, instabilities occur [1–3], or localization may be destroyed [4]. In the experiments studying the localization properties of matter waves in speckle potentials [5], the nonlinear regime, arising from the atomic interactions, is almost unavoidable. Furthermore, nonlinear behavior is easily observed in coherent backscattering (CBS) experiments with cold atomic gases [6]. Also random lasers exhibit nonlinearities which potentially influence the structure of localized laser modes [7]. In all these cases, even if the systems are governed by simple nonlinear wave equations, a precise description of the impact of this nonlinearity on the interference effects altering the properties of diffuse wave propagation is still lacking. Since exact numerical calculations for realistic situations are at the border of or beyond actual computer capacities, one needs an efficient theory providing directly disorder averaged quantities. For this purpose, the present Letter shows that the standard diagrammatic approach [8] can be extended to the nonlinear regime. Using ladder and crossedlike diagrams, we will derive a nonlinear radiative transfer equation for the averaged wave intensity and then calculate the interference corrections on top of the nonlinear solution.

The general framework for our approach is as follows: we assume a nonlinear wave equation with unique and stationary monochromatic solution, meaning, in particular, that the nonlinear susceptibilities at harmonics frequencies are weak enough such that the latter can be neglected. We also neglect—on the length scale ℓ (mean free path) set by the disorder—effects like self-focusing, pattern formation, and solitons [9], which originate from nonlinear variations Δn_{nl} of the real part of the refractive index. This assumption is valid if $(\Delta n_{\mathrm{nl}})^2 k\ell \ll 1$ [2]. Our theory also applies to imaginary Δn_{nl}, i.e., absorbing or amplifying media, provided, in the latter case, that the solutions remain stable. Within this general scenario, comprising examples like a collection of resonant point scatterers, or a (mean field) matter wave in a disordered potential, the nonlinear effects relevant in connection with the disorder are as follows: first, the wave intensity $I(\mathbf{r})$ becomes a fluctuating quantity, which is especially important in the nonlinear regime; second, the usual picture of weak localization resulting from interference only between pairs of amplitudes propagating along reversed paths breaks down in the nonlinear regime. As a consequence of nonlinear mixing between different partial waves, weak localization must rather be interpreted as a multiwave interference phenomenon [10,11]. In particular, we will show that the height of the coherent backscattering peak is strongly affected by nonlinearities, even if they do respect the reciprocity symmetry. In contrast to [10,11], the present approach is valid in the nonperturbative regime of arbitrarily large scattering media, where expansions in powers of the nonlinearity strength do not converge and even small nonlinearities may have a large impact on the wave propagation.

At first, we consider an assembly of N pointlike scatterers located at randomly chosen positions $\mathbf{r}_i$, $i = 1, \ldots, N$ inside a sample volume V illuminated by a plane wave $\mathbf{k}_L$. We assume the field radiated by each scatterer to be a nonlinear function $f(E_i)$ of the local field E_i. Neglecting higher harmonics, we write $f(E) = g(I)E$, where $I = EE^*$ is the local intensity, and $g(I)$ is proportional to the polarizability of the scatterers. This results in a set of nonlinear equations for the field at each scatterer:

$$E_i = e^{i\mathbf{k}_L\cdot\mathbf{r}_i} + \sum_{j\neq i} \frac{e^{ik|\mathbf{r}_i-\mathbf{r}_j|}}{4\pi|\mathbf{r}_i-\mathbf{r}_j|}\, g(E_jE_j^*)E_j, \qquad (1)$$

where $k = |\mathbf{k}_L|$, and the field is measured in units of the incident plane wave amplitude. For simplicity, we will consider only scalar fields in this Letter.

We aim at providing a theory providing the relevant quantities (local intensities, CBS cone, etc.) averaged over the random positions of the scatterers. In a first step, we will derive an equation for the mean intensity $\langle I(\mathbf{r})\rangle$. In the dilute regime, where the typical distances $|\mathbf{r}_i - \mathbf{r}_j|$ are much larger than the wavelength, we may neglect correlations between the fields emitted by different scatterers. The scattered field $E_d(\mathbf{r})$ is then a superposition of spherical

waves with random relative phases, depicting thus a speckle pattern. The resulting Gaussian statistics for the complex field $E_d(\mathbf{r})$ [12] are completely determined by a single parameter, the mean diffuse intensity $I_d(\mathbf{r}) = \langle |E_d(\mathbf{r})|^2 \rangle$. In addition to the scattered field, there is also a nonfluctuating coherent component originating directly from the incident field. In total, we have $E(\mathbf{r}) = \langle E(\mathbf{r}) \rangle + E_d(\mathbf{r})$, and the average intensity splits into a coherent and diffuse part: $\langle I(\mathbf{r}) \rangle = I_c(\mathbf{r}) + I_d(\mathbf{r})$, with $I_c = |\langle E \rangle|^2$. The mean density of radiation intensity emitted from point $\mathbf{r}$ is then given by

$$K(\mathbf{r}) = \mathcal{N} \langle f f^* \rangle = \mathcal{N} \langle |g(I(\mathbf{r}))|^2 I(\mathbf{r}) \rangle, \tag{2}$$

where $\mathcal{N} = N/V$ denotes the density of scatterers, and the average $\langle \ldots \rangle$ is taken over the Gaussian statistics of the scattered field.

Between two scattering events, the wave propagates in an effective medium made by the scatterers, described by a refractive index n and mean free path ℓ. Note that, because of the nonlinear behavior of the scatterers, the effective medium is modified by the propagating waves themselves. Because of their different statistical properties, we obtain therefore different refractive indices for coherent and diffuse fields, respectively. (This effect is also known from usual pump-probe configurations in nonlinear optics [9].) In the dilute regime, the diffuse amplitude can be considered as a weak probe, such that the complex refraction index reads as follows:

$$n = 1 + \frac{\mathcal{N}}{2k^2} \left\langle \frac{df}{dE} \right\rangle, \qquad \frac{1}{\ell} = 2k \mathrm{Im}\{n\}, \tag{3}$$

whereas, for the coherent mode, the derivative d/dE is replaced by $1/\langle E \rangle$; i.e., $n_c = 1 + \mathcal{N} \langle f \rangle / (2k^2 \langle E \rangle)$, and $1/\ell_c = 2k \mathrm{Im}\{n_c\}$. Since the results of the averages depend on $I_c(\mathbf{r})$ and $I_d(\mathbf{r})$, the nonlinear refractive indices also attain a spatial dependence $n(\mathbf{r})$ and $n_c(\mathbf{r})$. They describe average propagation of one strong and many uncorrelated weak fields.

Recollecting all preceding ingredients, the transport equations for the average intensity read as follows:

$$I_c(\mathbf{r}) = e^{-\overline{z/\ell_c}}, \tag{4}$$

$$I_d(\mathbf{r}) = \int_V d\mathbf{r}' \frac{e^{-\overline{|\mathbf{r}-\mathbf{r}'|/\ell}}}{(4\pi |\mathbf{r}-\mathbf{r}'|)^2} K(\mathbf{r}'). \tag{5}$$

Here, z denotes the distance from the surface of V to $\mathbf{r}$, in the direction of the incident beam. Furthermore, propagation from $\mathbf{r}'$ to $\mathbf{r}$ implies a spatial average of $1/\ell(\mathbf{r})$, which we note as $\overline{|\mathbf{r}-\mathbf{r}'|/\ell} := |\mathbf{r}-\mathbf{r}'| \int_0^1 ds/\ell(\mathbf{r} - s\mathbf{r} + s\mathbf{r}')$, and similarly for $\overline{(z/\ell_c)}$. Since K, ℓ, and ℓ_c depend on $I_c(\mathbf{r})$ and $I_d(\mathbf{r})$, the above Eqs. (4) and (5) form two coupled integral equations. Finally, the intensity scattered into backwards direction, expressed by the "bistatic coefficient" [8], results as

$$\Gamma_L = \int_V \frac{d\mathbf{r}}{4\pi A} e^{-\overline{z/\ell}} K(\mathbf{r}), \tag{6}$$

where A denotes the transverse (with respect to the incident beam) area of the scattering volume V.

The validity of the preceding approach has been tested using the nonlinear function $g(I) = (4\pi i)/k(1 + \alpha I)$ which depicts the (elastic) nonlinear behavior of a two-level atom exposed to an intense laser beam. We must emphasize that, for this particular model of nonlinearity, the stationary solution is always found to be unique and stable, as a consequence of the saturation $g(I) \to 0$ for large α. From the numerical solution of Eq. (1), we calculate the radiated intensity outside the cloud in different directions θ. This procedure is then repeated with many different configurations giving us the disorder averaged field and intensity. The results presented in this Letter are obtained with 3000 configurations of 1500 scatterers, randomly distributed inside a sphere with a homogeneous density ($k\ell = 67$ and optical thickness $b = 2$ for $\alpha = 0$).

The results for the average intensity as a function of the backscattering angle θ are depicted in Fig. 1 for different values of the nonlinear parameter $\alpha = 0$, 0.2, 0.4, and 0.6. For each plot, the solid line depicts the exact numerical results, whereas the dashed line corresponds to Γ_L, Eq. (6). Away from the backward direction, the agreement between the exact numerical calculations and our theoretical prediction for the background is clearly excellent. This is emphasized by the additional curve (long dashed line)

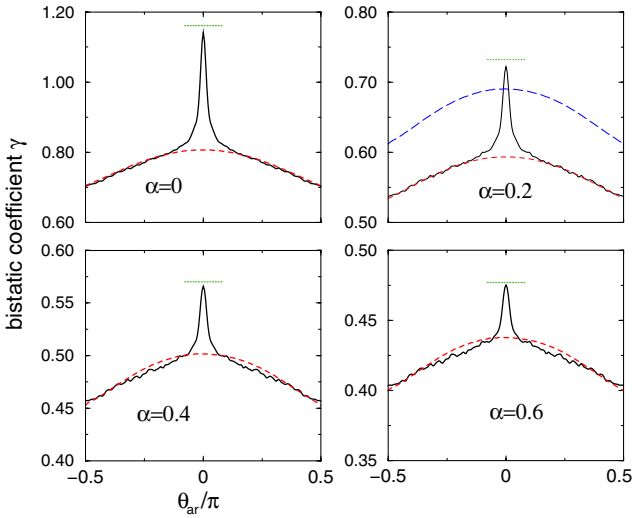

FIG. 1 (color online). Coherent backscattering cones obtained from exact numerical calculations in comparison to the theoretical approach, for various nonlinearity strengths α. The solid lines depict the exact numerical results, whereas the dashed lines correspond to Γ_L including geometrical effects. The dotted lines correspond to the sum $\Gamma_L + \Gamma_C$ exactly in the backward direction. The additional curve (long dashed line) plotted for $\alpha = 0.2$ depicts Γ_L obtained when the fluctuating character of the diffuse field is not taken into account.

plotted for $\alpha = 0.2$ depicting the results obtained when neglecting the fluctuations of $I(\mathbf{r})$, for example, replacing $\langle |g(I)|^2 I\rangle$ by $|g(\langle I\rangle)|^2\langle I\rangle$ in Eq. (2).

In the backward direction, constructive interference between reversed scattering paths results in the well-known coherent backscattering peak. As is obvious from Fig. 1, the height of this peak is strongly reduced by the nonlinearity. Nevertheless, we are perfectly able to incorporate these interference effects in our approach, see the horizontal dotted lines in Fig. 1, which depict the predicted total bistatic coefficient, $\Gamma_L + \Gamma_C$, see Eq. (12) below, in the exact backward direction. These results are obtained by a diagrammatic analysis, whose results we briefly outline in the following. A detailed derivation will be presented elsewhere.

In contrast to a previous attempt for a nonlinear diagrammatic theory [13], we concentrate on the regime $k\ell \gg 1$ of dilute media, which allows us to sum up the diagrammatic series in a simple, closed form, as shown below. As for linear media in the dilute regime, we calculate the CBS effect by so-called ''crossed'' or ''Cooperon'' diagrams [8], describing pairs of reversed scattering paths. As a first step, we analyze how a single scatterer responds to two different incident probe fields E and E^*, which represent the two amplitudes propagating along the reversed paths. Note that, due to the nonlinearity, the scattered field f and its complex conjugate f^* depend on both E and E^*. Hence, depending on whether the probe fields act on f or f^*, we obtain the building blocks depicted in Fig. 2. Expressing, as in Eq. (3), the scatterer's response to a small probe field by d/dE (or d/dE^*), the corresponding mathematical expressions read

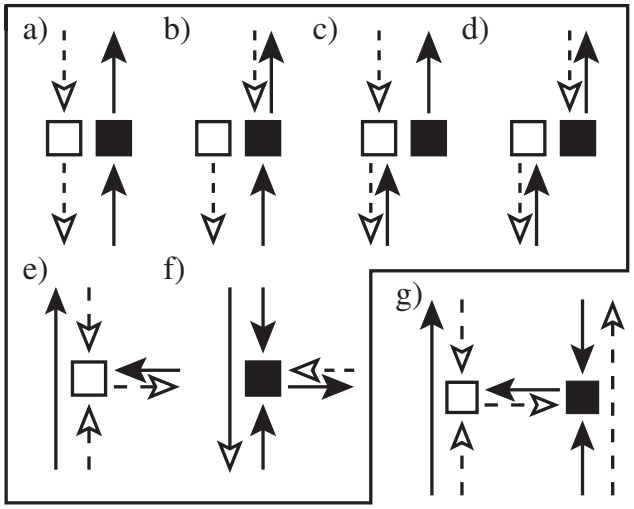

FIG. 2. (a)–(f) Building blocks for the diagrammatic calculation of nonlinear CBS. Filled squares (with outgoing solid arrows) denote the scattered field f, and open squares (with outgoing dashed arrows) the complex conjugate f^*. Incoming solid (dashed) arrows represent probe fields d/dE (d/dE^*). (g) Example of a forbidden combination of diagrams, exhibiting a closed loop (see the main text).

$$\kappa = \mathcal{N}\left\langle \frac{d}{dE}\left(f\frac{df^*}{dE^*}\right)\right\rangle, \qquad \tilde{\kappa} = \mathcal{N}\left\langle \frac{d}{dE}\left(f^*\frac{df}{dE^*}\right)\right\rangle, \quad (7)$$

where κ represents the sum of diagram (a) + (c), $\tilde{\kappa}$ the sum (b) + (d), and

$$\tau = -\frac{i\mathcal{N}}{2k}\left\langle \frac{d^3 f^*}{(dE^*)^2 dE}\right\rangle \quad (8)$$

diagram (e). If one of the incident fields originates from the coherent mode, d/dE is again replaced by $1/\langle E\rangle$; i.e., $\kappa_c = \mathcal{N}\langle f\, df^*/dE^*\rangle/\langle E\rangle$, $\tilde{\kappa}_c = \mathcal{N}\langle f^*\, df/dE^*\rangle/\langle E\rangle$, and $\tau_c = -i\mathcal{N}\langle d^2 f^*/(dE^*)^2\rangle/(2k\langle E\rangle)$.

In the next step, the crossed transport equation is established by connecting the building blocks shown in Fig. 2 with each other. However, there are some combinations of diagrams, for example, the one shown in Fig. 2(g), which represent unphysical processes. In this diagram the fields radiated by f^* and f mutually depend on one another, and, therefore, one cannot tell which one of the two events f or f^* happens before the other one. In order to avoid closed loops like the one shown in Fig. 2(g), we ignore all combinations where one of the diagrams Fig. 2(c), 2(d), or 2(e) occurs after Fig. 2(b), 2(d), or 2(f) when following the solid arrow along the crossed path.

We account for these forbidden diagrams by splitting the transport equation into two parts, which we call C_1 and C_2. The first part, C_1, contains only diagrams Figs. 2(a), 2(c), and 2(e). As soon as one of the events Fig. 2(b), 2(d), or 2(f) occurs, the crossed intensity changes from type C_1 to type C_2. The subsequent propagation of C_2 is then given by diagrams Figs. 2(a), 2(b), and 2(f). Following these rules, we describe the propagation of $C_{1,2}$ by transport equations similar to Eqs. (4) and (5):

$$C_c(\mathbf{r}) = e^{ikz\overline{(n_c - n^*)}}, \quad (9)$$

$$C_1(\mathbf{r}) = \int_V d\mathbf{r}' P(\mathbf{r},\mathbf{r}')(\sigma C_1 + \sigma_c C_c)(\mathbf{r}'), \quad (10)$$

$$C_2(\mathbf{r}) = \int_V d\mathbf{r}' P(\mathbf{r},\mathbf{r}')(\sigma^* C_2 + \tilde{\sigma} C_1 + \tilde{\sigma}_c C_c)(\mathbf{r}'), \quad (11)$$

where $P(\mathbf{r},\mathbf{r}') = \exp(-\overline{|\mathbf{r}-\mathbf{r}'|/\ell})/(4\pi|\mathbf{r}-\mathbf{r}'|)^2$ is the same as in Eq. (5), and the cross sections σ result as follows: $\sigma = \kappa + \ell K\tau$, $\tilde{\sigma} = \tilde{\kappa} + \ell K\tau^*$, and, similarly, $\sigma_c = \kappa_c + \ell K\tau_c$ and $\tilde{\sigma}_c = \tilde{\kappa}_c + \ell K\tau_c^*$. Finally, the crossed bistatic coefficient reads

$$\Gamma_C = \int_V \frac{d\mathbf{r}}{4\pi A} e^{ikz\overline{(n-n_c^*)}}[(\sigma_c^* + \tilde{\sigma}_c^*)C_1 + \sigma_c^* C_2](\mathbf{r}). \quad (12)$$

For comparison with the background Γ_L, we define diffuson cross sections by writing $K = \sigma^{(d)} I_d + \sigma_c^{(d)} I_c$, such that Eq. (5) attains a form comparable to Eq. (10).

Exploiting the Gaussian properties of the diffuse field, we find $\sigma^{(d)} = \sigma - \tilde{\sigma}^*$ and $\sigma_c^{(d)} = \sigma_c - \tilde{\sigma}_c^*$.

How the nonlinearity affects the CBS effect can now be understood by comparing σ and $\sigma^{(d)}$. For the case of an absorbing nonlinearity, we find $\tilde{\sigma} < 0$, and hence $\sigma < \sigma^{(d)}$. Consequently, the crossed intensity is absorbed more strongly than the background intensity, which explains the decrease of the CBS cone observed in Fig. 1. Let us note that there also exist other models, for example, an amplifying nonlinearity like $g = 4\pi i(1 + \alpha I)/k$, where our theory predicts an enhancement of the CBS cone. However, these models might suffer from instabilities, requiring thus further investigations.

To obtain the relatively simple form of Eqs. (9)–(12), we have performed some approximations valid in the case of large optical thickness b. In the numerical comparison depicted in Fig. 1, we have used the exact version of Eqs. (9)–(12), which will be published elsewhere.

As explained in the introduction, our theoretical scheme also applies to other types of nonlinear systems. Instead of a collection of nonlinear scatterers as described by Eq. (1), we may, for example, also consider linear scatterers embedded in a homogeneous nonlinear medium:

$$\Delta E(\mathbf{r}) + k^2[\epsilon(\mathbf{r}) + \alpha|E(\mathbf{r})|^2]E(\mathbf{r}) = 0 \qquad (13)$$

with δ-correlated disorder $\epsilon(\mathbf{r})$ corresponding to a (linear) mean free path ℓ_0. Here, the dilute medium approximation is valid if $k\ell_0 \gg 1$ and $(\alpha I)^2 k\ell_0 \ll 1$. The latter condition is automatically fulfilled if we assume that we are in the stable regime, where Eq. (13) has a unique solution. According to [2], this is the case (for $\alpha \in \mathbb{R}$) if $(\alpha I)^2 b^2(k\ell_0 + b) < 1$, with b the optical thickness.

In this case, the diagrammatic method applies in the same way as described above. In particular, we obtain the following expressions for the cross sections:

$$\sigma(\mathbf{r}) = \sigma_c(\mathbf{r}) = \frac{4\pi}{\ell_0}\{1 + ik\ell_0\alpha[I_c(\mathbf{r}) + I_d(\mathbf{r})]\}, \qquad (14)$$

$\tilde{\sigma} = \tilde{\sigma}_c = -4\pi ik\alpha^*(I_c + I_d)$, $\sigma^{(d)} = \sigma_c^{(d)} = 4\pi/\ell_0$, and for the mean free paths $n = \langle\epsilon\rangle + \alpha(I_c + I_d) + i/(2k\ell_0)$ and $n_c = \langle\epsilon\rangle + \alpha(I_c/2 + I_d) + i/(2k\ell_0)$. In the energy conserving case $\alpha \in \mathbb{R}$, it can be shown that C_2 does not contribute to the real part of the backscattering coefficient Γ_C. Since, in this case, the Cooperon cross section, Eq. (14), exhibits a complex phase factor, it follows from Eq. (10) that the nonlinearity introduces a phase difference $\Delta\phi = Mk\ell_0\alpha I$ between reversed paths undergoing M linear scattering events. Since $\langle M\rangle \propto b$, we predict a significant reduction of the CBS peak if $bk\ell_0\alpha I \simeq 1$ (which is still inside the stable regime if $k\ell_0$ is large).

In summary, we have extended the usual diagrammatic approach to take into account nonlinear effects for the coherent transport in disordered systems beyond the perturbative regime. The excellent agreement with direct numerical simulations emphasizes the validity of our approach. It readily applies for different nonlinear wave equations. Equation (13), for example, is mathematically equivalent to the Gross-Pitaeskii equation describing nonlinear propagation of matter waves in random potentials. In this case, our method will allow us to describe not only the localization properties of the mean field, but also, extending it within the Bogoliubov framework, the effect of the noncondensed atoms. Furthermore, nonlinear transport of light in cold atomic gases [6] can be described by including inelastic scattering (Mollow's triplet). Finally, our present theory, combined with the usual self-consistent approach of strong localization [14], can possibly allow a quantitative understanding of the impact of the nonlinearity in the strong scattering regime.

We thank D. Delande and C. Miniatura for fruitful discussions. T. W. acknowledges support from the DFG.

[1] B. Spivak and A. Zyuzin, Phys. Rev. Lett. **84**, 1970 (2000).
[2] S. E. Skipetrov and R. Maynard, Phys. Rev. Lett. **85**, 736 (2000).
[3] T. Paul *et al.*, Phys. Rev. A **72**, 063621 (2005).
[4] D. L. Shepelyansky, Phys. Rev. Lett. **70**, 1787 (1993).
[5] D. Clément *et al.*, Phys. Rev. Lett. **95**, 170409 (2005); C. Fort *et al.*, Phys. Rev. Lett. **95**, 170410 (2005); T. Schulte *et al.*, Phys. Rev. Lett. **95**, 170411 (2005).
[6] T. Chanelière *et al.*, Phys. Rev. E **70**, 036602 (2004); S. Balik *et al.*, J. Mod. Opt. **52**, 2269 (2005).
[7] H. Cao, Waves Random Media **13**, R1 (2003).
[8] M. B. van der Mark, M. P. van Albada, and A. Lagendijk, Phys. Rev. B **37**, 3575 (1988).
[9] R. W. Boyd, *Nonlinear Optics* (Academic, San Diego, 1992).
[10] T. Wellens *et al.*, Phys. Rev. E **71**, 055603(R) (2005); Phys. Rev. A **73**, 013802 (2006).
[11] T. Wellens and B. Grémaud, J. Phys. B **39**, 4719 (2006).
[12] J. W. Goodman, J. Opt. Soc. Am. **66**, 1145 (1976).
[13] A. J. van Wonderen, Phys. Rev. B **50**, 2921 (1994).
[14] D. Vollhardt and P. Wölfle, Phys. Rev. Lett. **48**, 699 (1982); S. E. Skipetrov and B. A. van Tiggelen, Phys. Rev. Lett. **96**, 043902 (2006).